MicroRNA-155 coordinates the immunological landscape within murine melanoma and correlates with immunity in human cancers

SUPPLEMENTARY FIGURES

H. Atakan Ekiz[1,2], Thomas B. Huffaker[1,2], Allie H. Grossmann[3,4,5], W. Zac Stephens[2], Matthew A. Williams[2], June L. Round[2] and Ryan M. O'Connell[2,*]

[2] Division of Microbiology and Immunology,

[3] Division of Anatomic Pathology Department of Pathology, University of Utah,
15 N. Medical Dr. East, JMRB, Salt Lake City, UT, 84112

[4] Huntsman Cancer Institute, University of Utah Health Sciences Center,
2000 Circle of Hope Drive, Salt Lake City, UT, 84112, USA

[5] ARUP Laboratories, University of Utah,
500 Chipeta Way, Salt Lake City, UT 84112, USA

* Direct all correspondence to: Ryan M. O'Connell (ryan.oconnell@path.utah.edu)

phone: (801) 213-4153

[1] equal contribution

Conflict of Interest statement: The authors have declared that no conflict of interest exists.

Running Title: scSeq defines miR-155's role in antitumor immunity

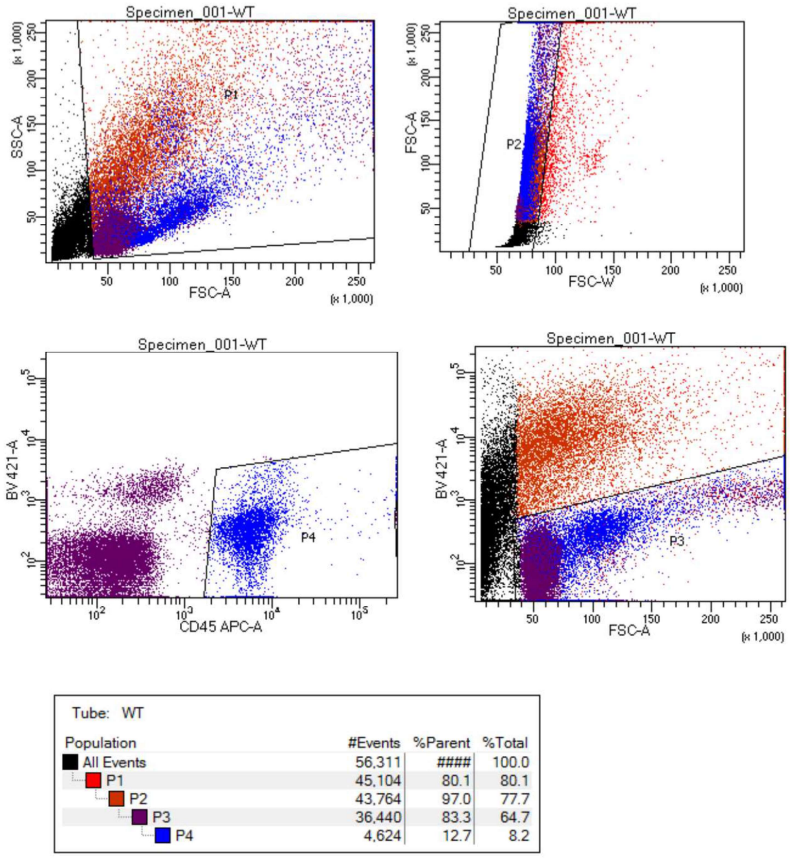

Tube: WT

Population	#Events	%Parent	%Total
All Events	56,311	####	100.0
P1	45,104	80.1	80.1
P2	43,764	97.0	77.7
P3	36,440	83.3	64.7
P4	4,624	12.7	8.2

Figure S1 – Flow cytometric sorting of tumor-infiltrating immune cells. Representative flow cytometry plots showing the methodology for sorting tumor infiltrating live immune cells as marked by CD45+DAPI- phenotype (blue color in dot plots).

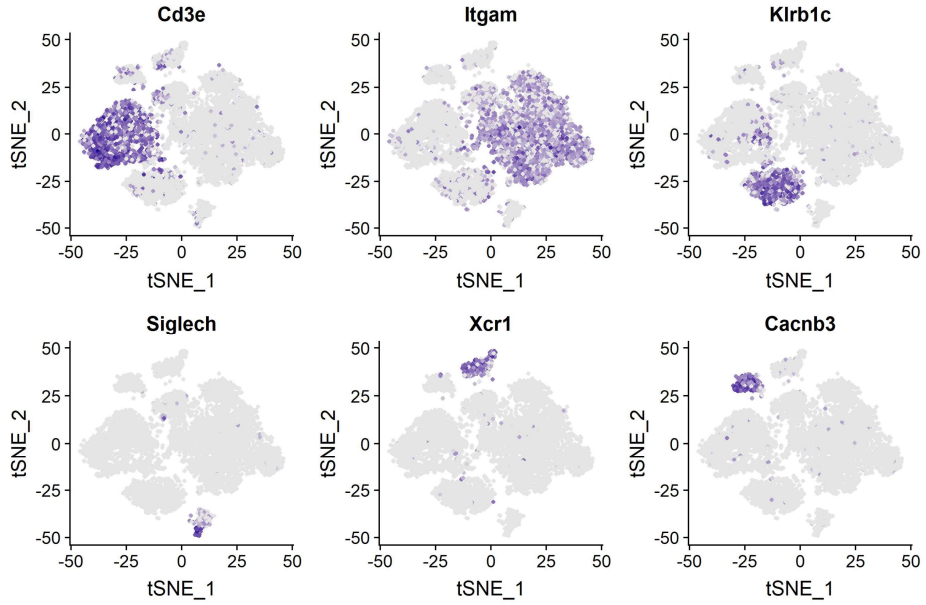

Figure S2 – Lineage markers reveal main cell clusters in SCseq. Visualization of select immune-related genes in t-SNE plots identifies broad cell clusters. *CD3e*, *Itgam*, *Klrb1c*, *Siglech*, *Xcr1*, and *Cacnb3* marks T cells, myeloid subsets, NK cells, plasmacytoid DCs, Xcr1+ DCs, and Langerhans cells respectively.

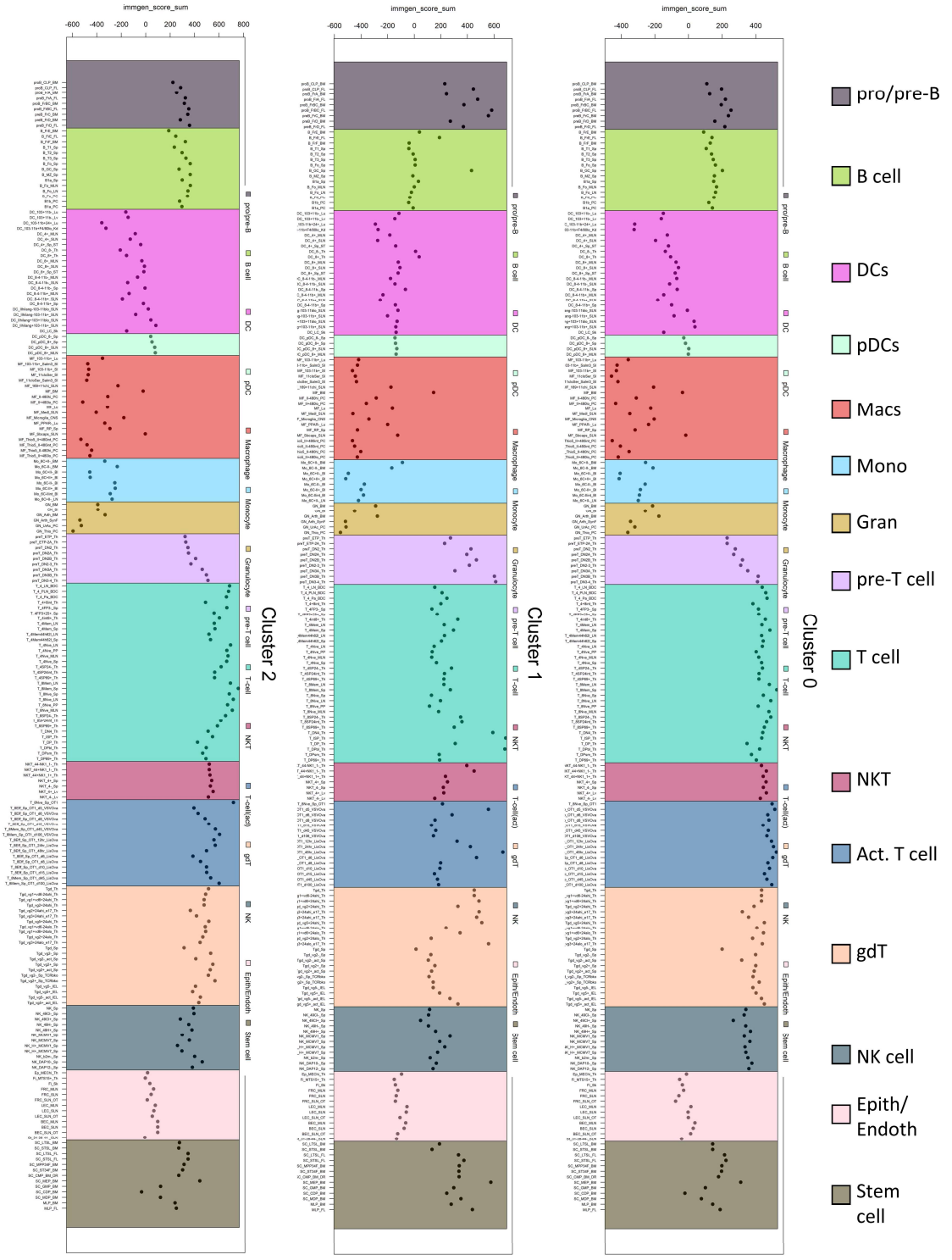

Figure S3 – A novel identity scoring algorithm assists in naming SCseq clusters. The output of immune cell scoring algorithm for each cluster is shown (see Methods). On the x-axis, ~200 cell subsets from the ImmGen database are listed. Y-axis indicates an aggregate score for each ImmGen subset for the cluster in the analysis. Graphs show the immune cell scores for each cluster in the SCseq data (Clusters 0-14 pre-naming). Top 5 highest scoring ImmGen subsets from these plots were plotted in Figure S4.

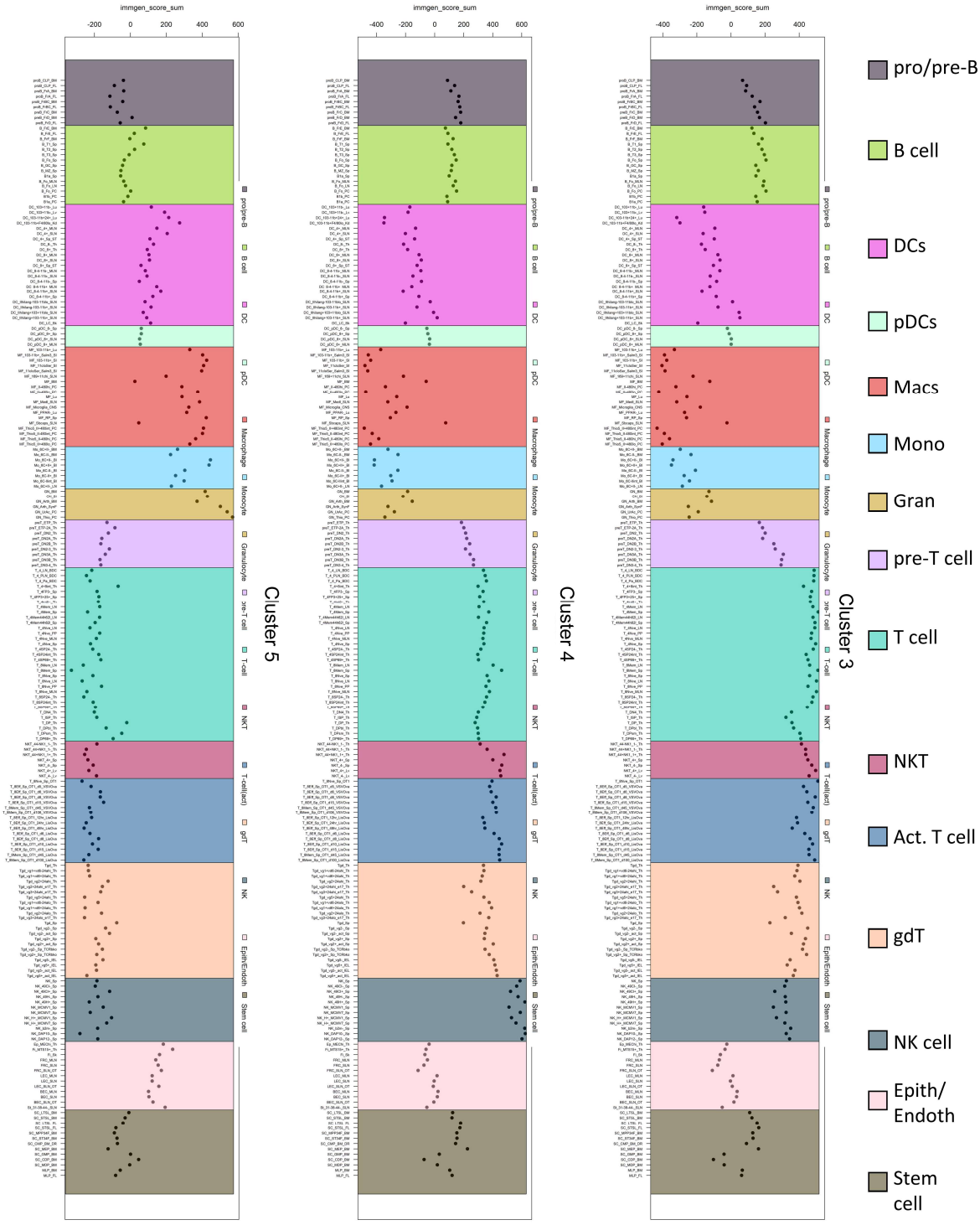

Figure S3 (cont'd)

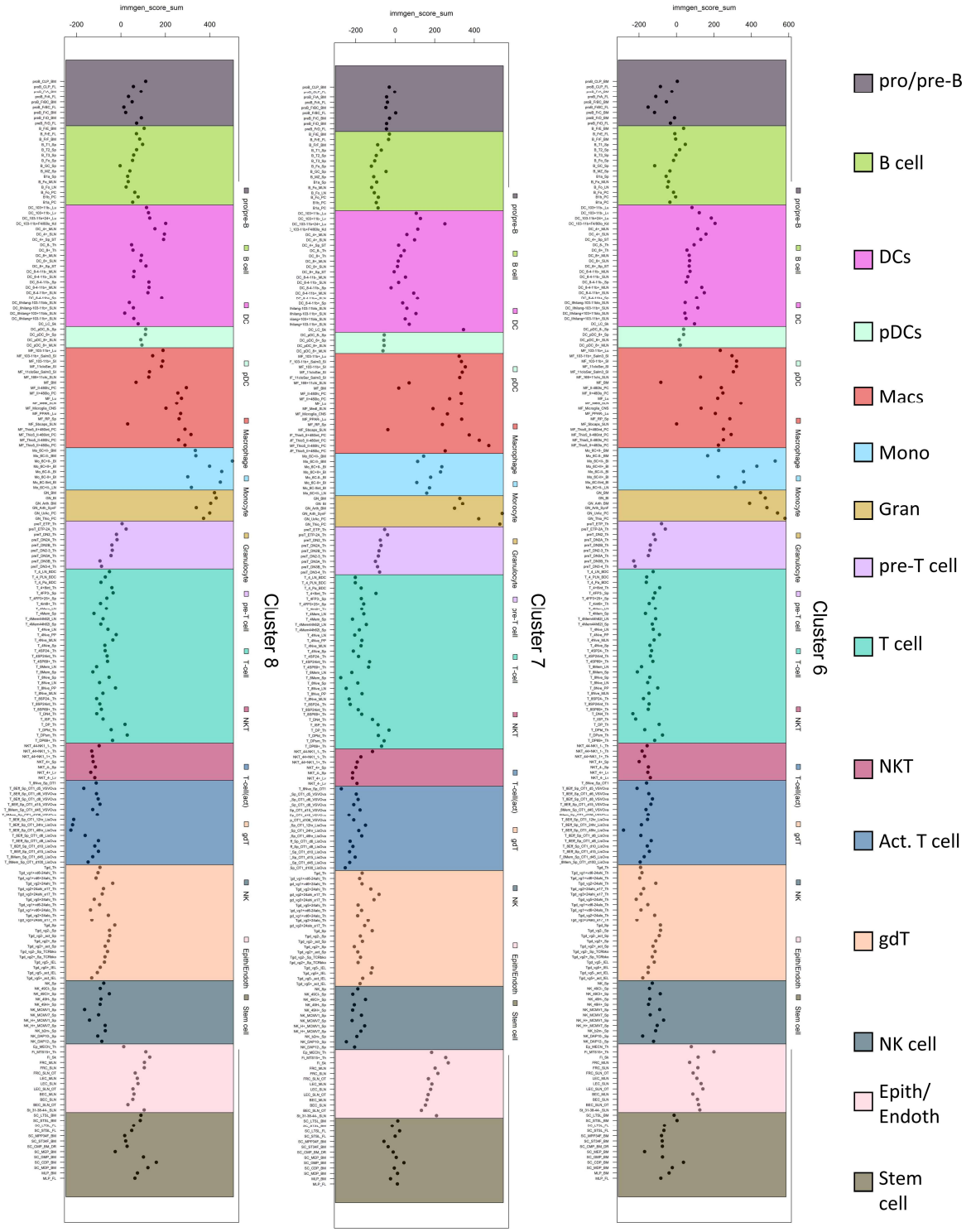

Figure S3 (cont'd)

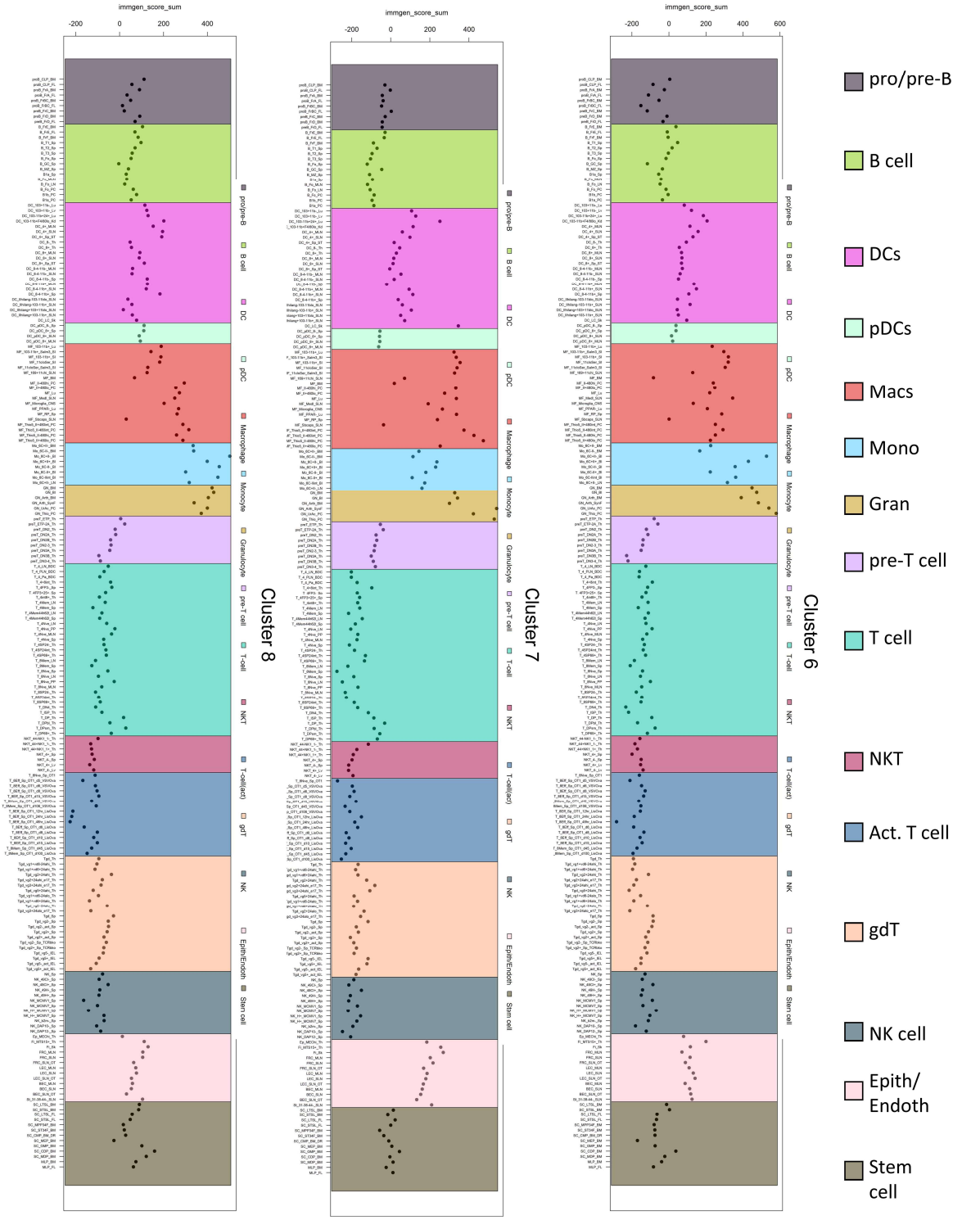

Figure S3 (cont'd)

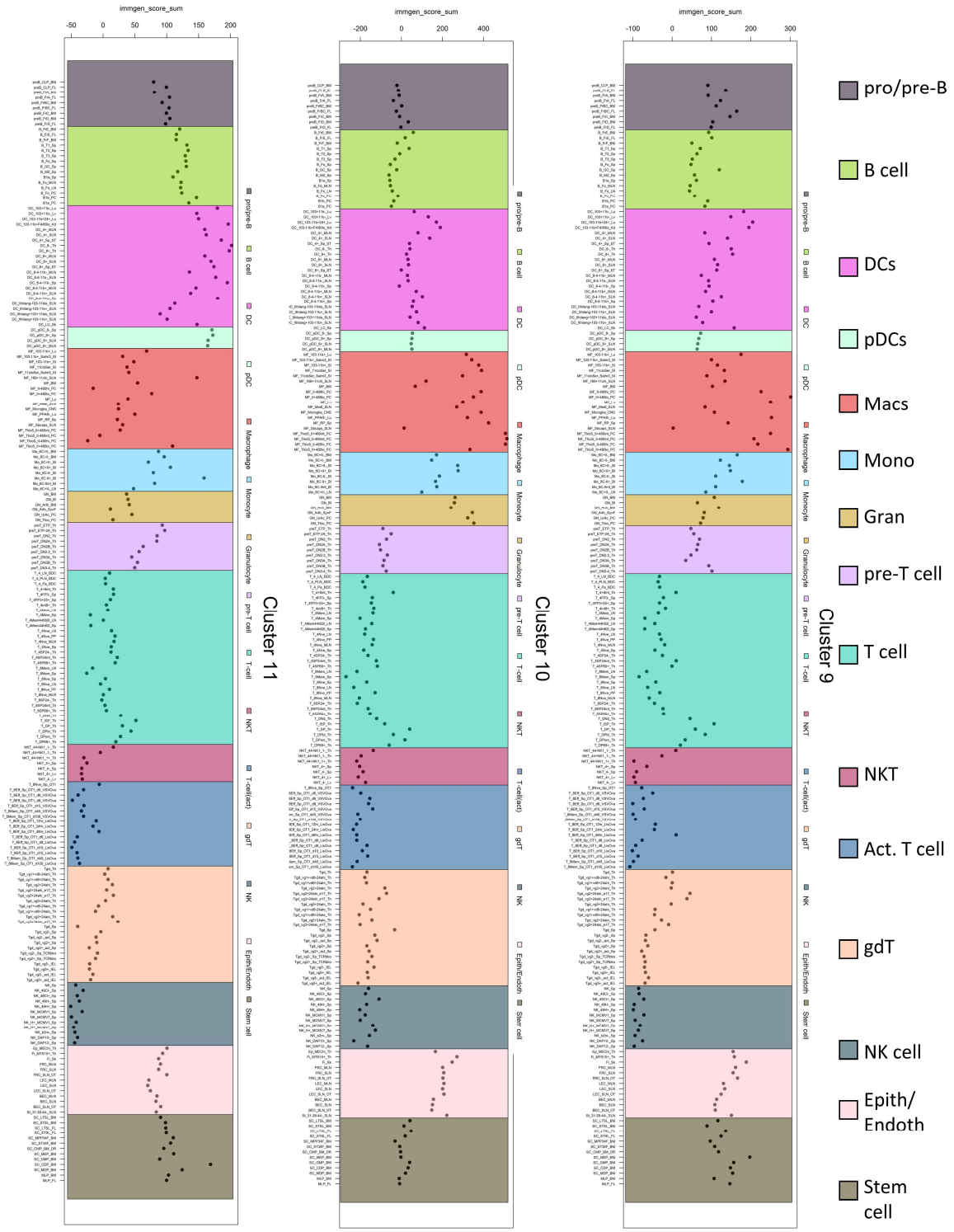

Figure S3 (cont'd)

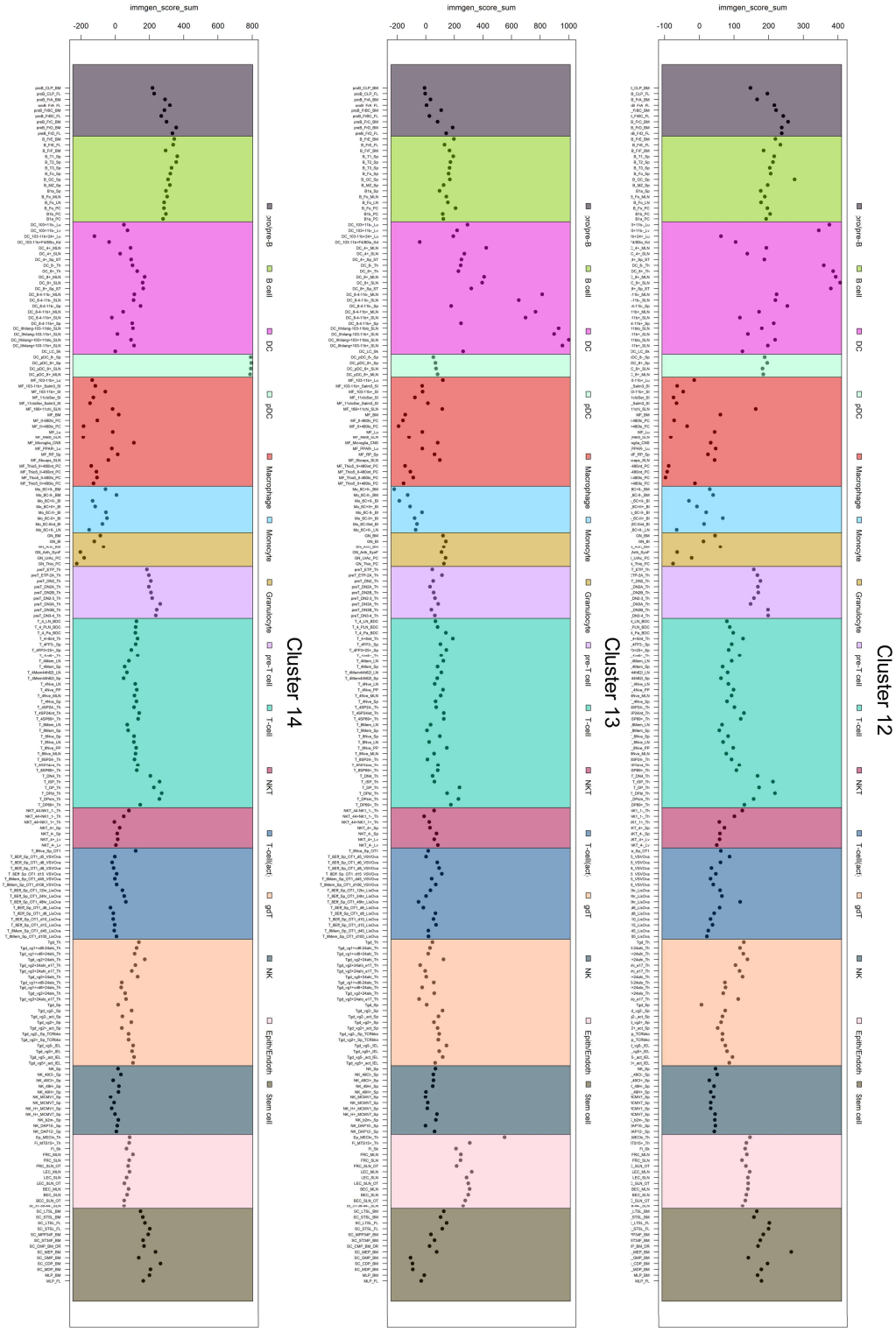

Figure S3 (cont'd)

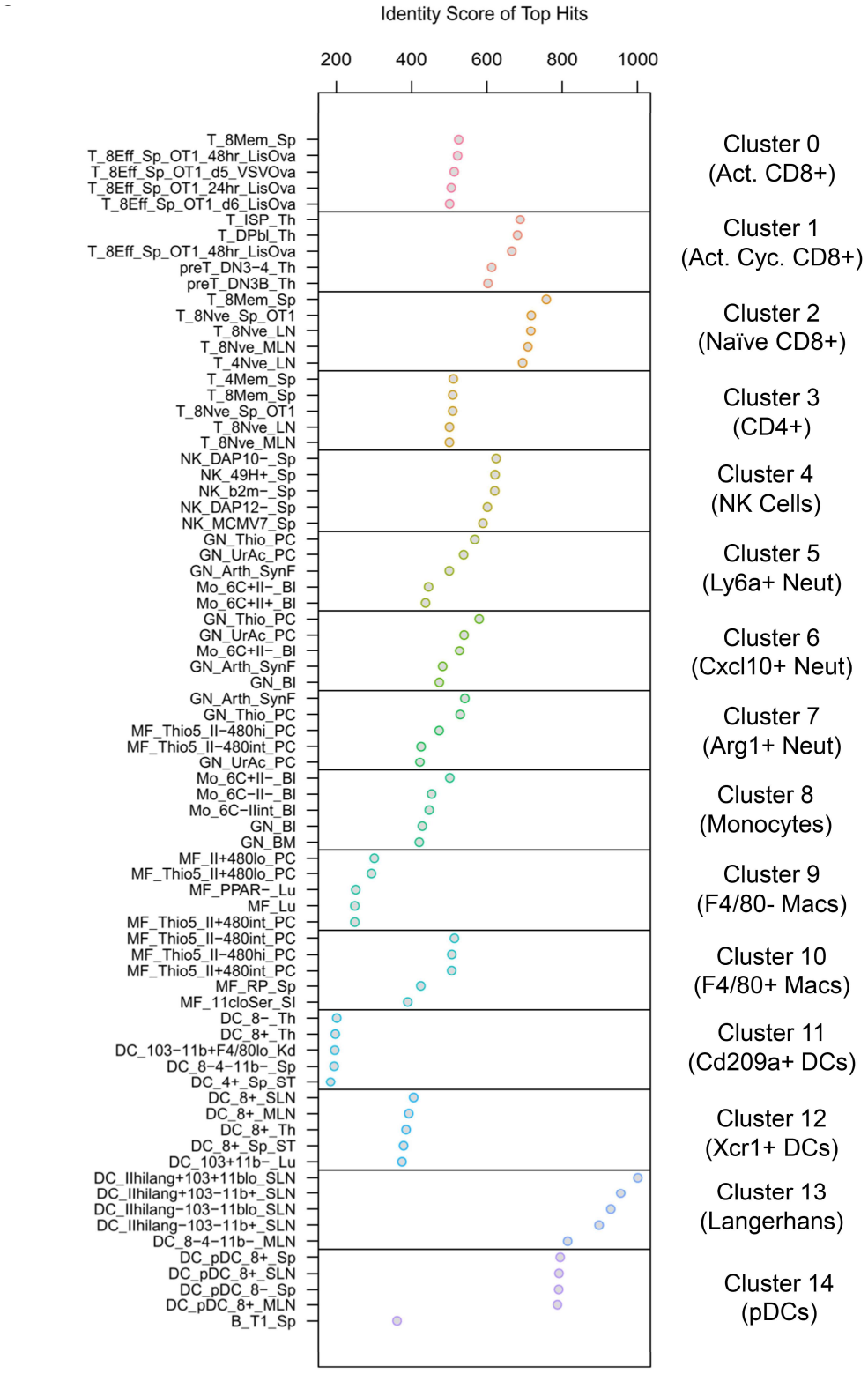

Figure S4 – Summary of top hits for each cluster calculated by identity scoring algorithm. Summary output of our immune cell scoring algorithm. Top 5 highest scoring immune cell subsets from the ImmGen database were plotted for each cluster. Clusters 0 to 13 were named as indicated by the help of this algorithm and differential expression analyses between closely related clusters.

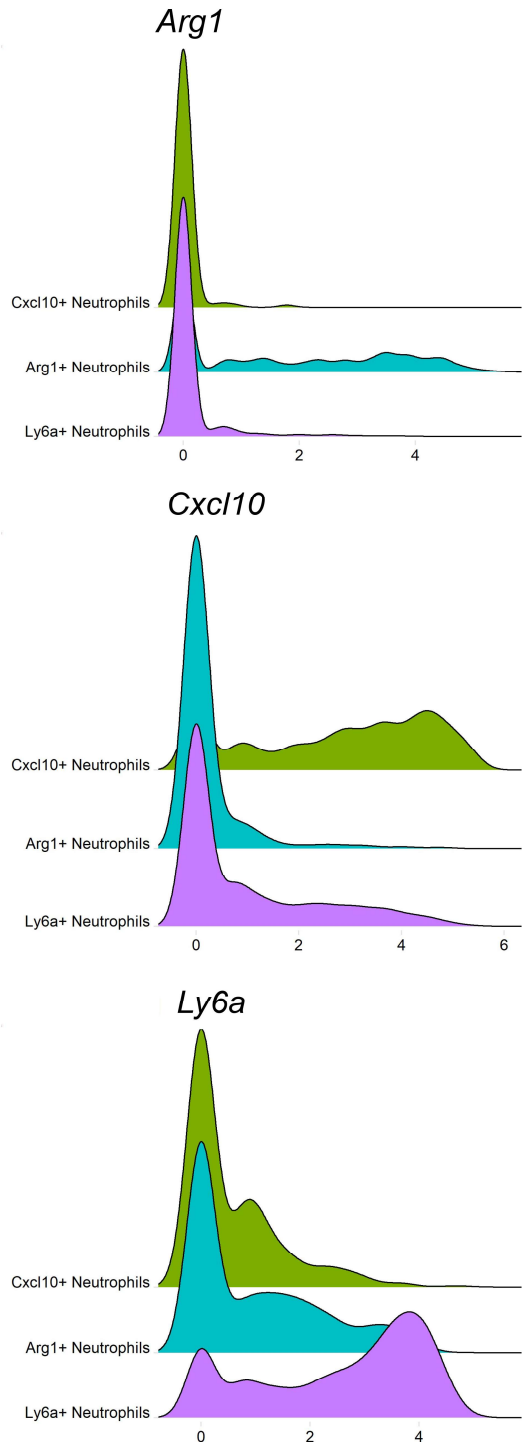

Figure S5 – Closely related neutrophil subsets can be distinguished based on differential gene expression. Expression of *Arg1*, *Cxcl10*, and *Ly6a* in three neutrophil clusters are shown. For this graph, data from WT and miR-155 TCKO samples on days 9 and 12 were combined. These genes are selected to distinguish neutrophil subsets since they showed a differential expression profile.

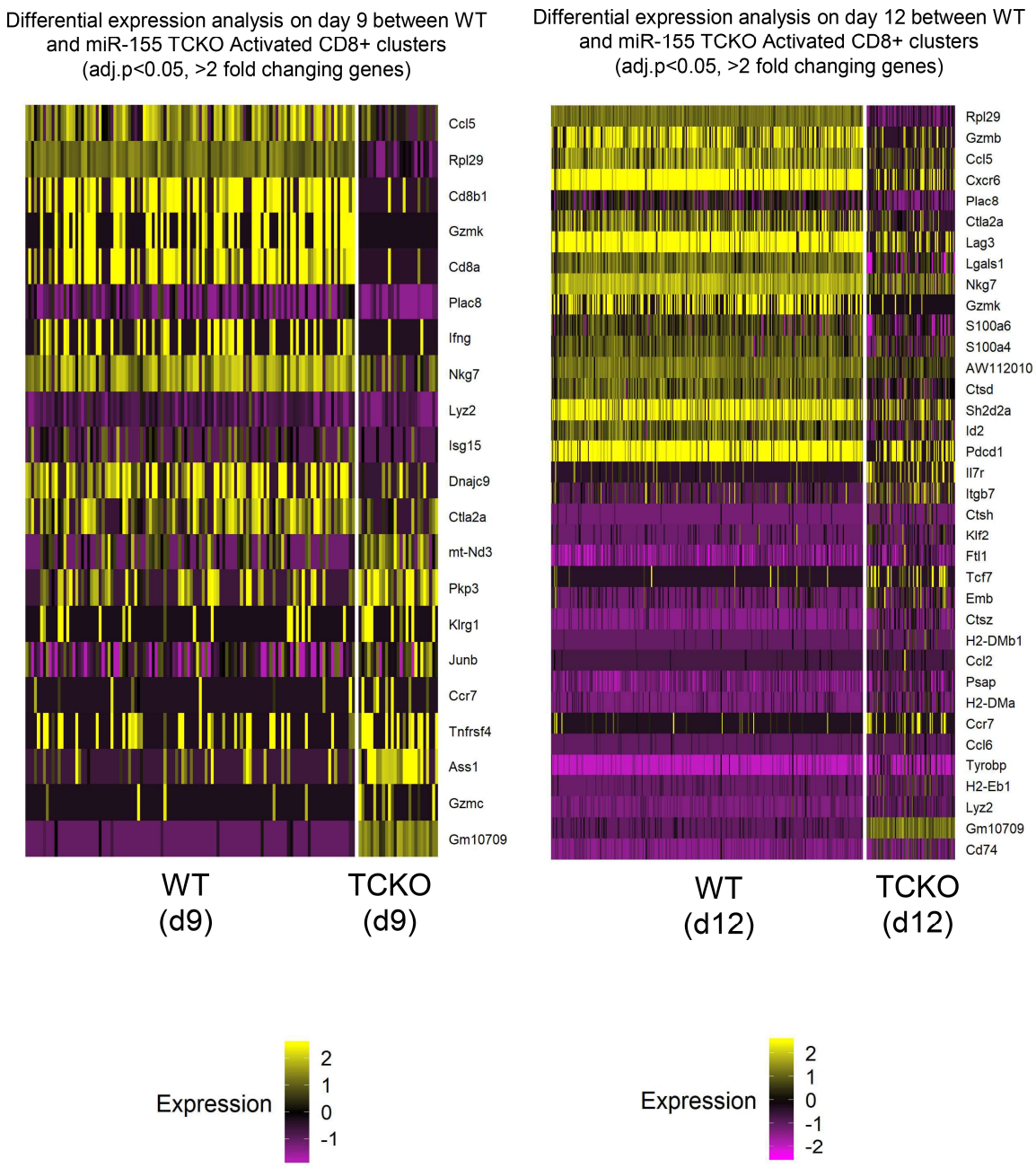

Figure S6 – Differential gene expression in activated CD8+ T cell clusters. Heatmaps showing differentially expressed genes in Activated CD8+ T cell clusters. WT and miR-155 TCKO samples were compared on days 9 and 12 separately. Genes shown in the heatmaps met the cut-off criteria of adjusted p-value of <0.05 and >2 linear fold-change.

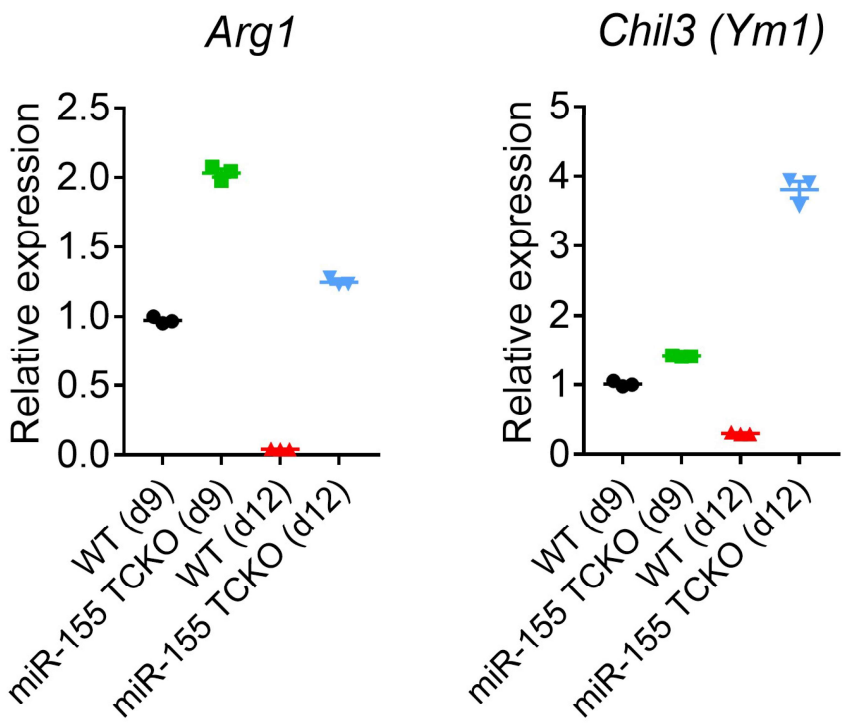

Figure S7 – qPCR validation of *Arg1* and *Chil3* differential expression. Plots validate the gene expression changes observed in SCseq data. For this experiment, RNA from sorted CD45+ tumor infiltrating leukocytes was used (pooled from 4 mice as indicated in Figure 1a, and in Methods section). qPCR reaction was performed in triplicates and each point indicates a technical replicate.

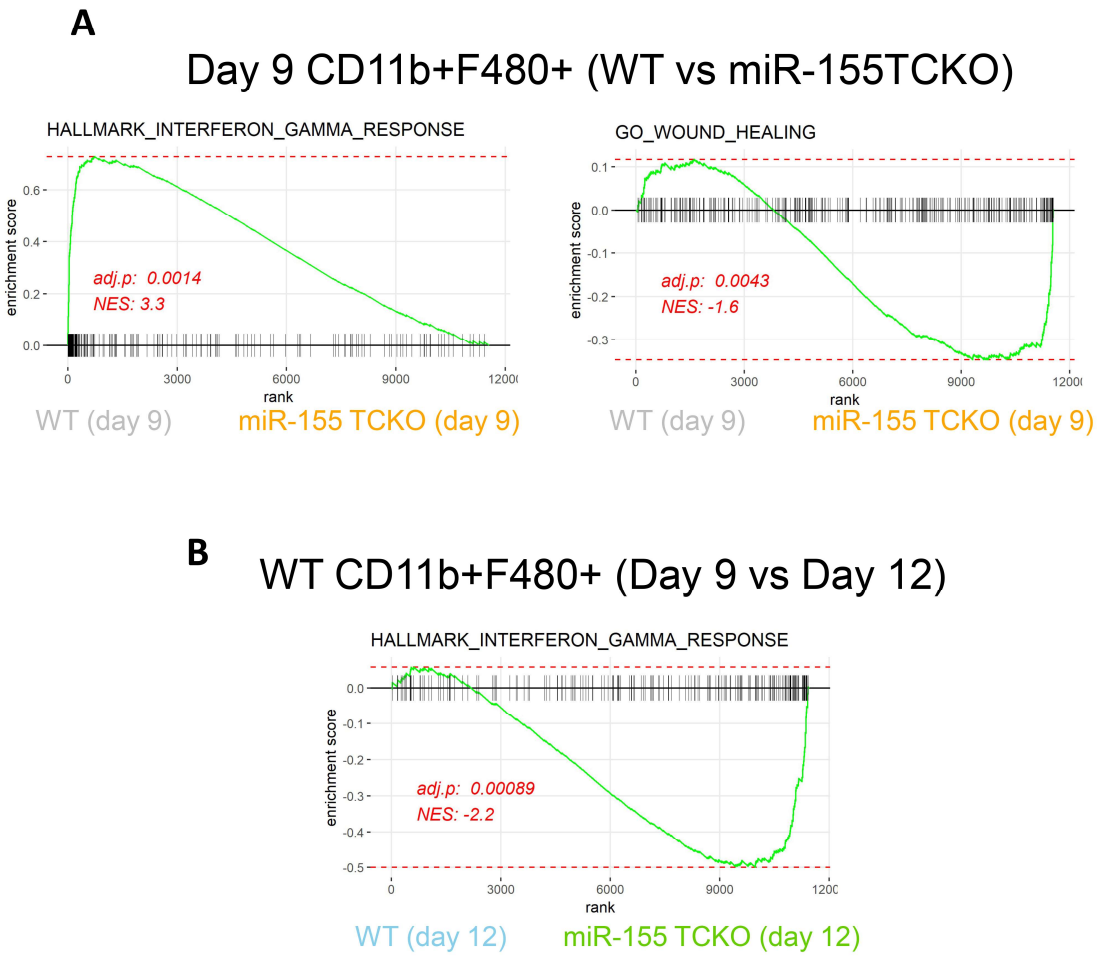

Figure S8 – GSEA of CD11b+F4/80+ macrophages in the TME. A. Comparison of WT and miR-155 TCKO macrophages on day 9 revealed an enrichment of IFNg response genes in WT samples and enrichment of wound healing genes in miR-155 TCKO counterparts. **B.** Comparison of gene set enrichment in WT macrophages between days 9 and 12 revealed an enrichment of IFNg response signature at the later time point suggesting an evolving antitumor immune response over time. Normalized enrichment score (NES) and adjusted p values are shown.

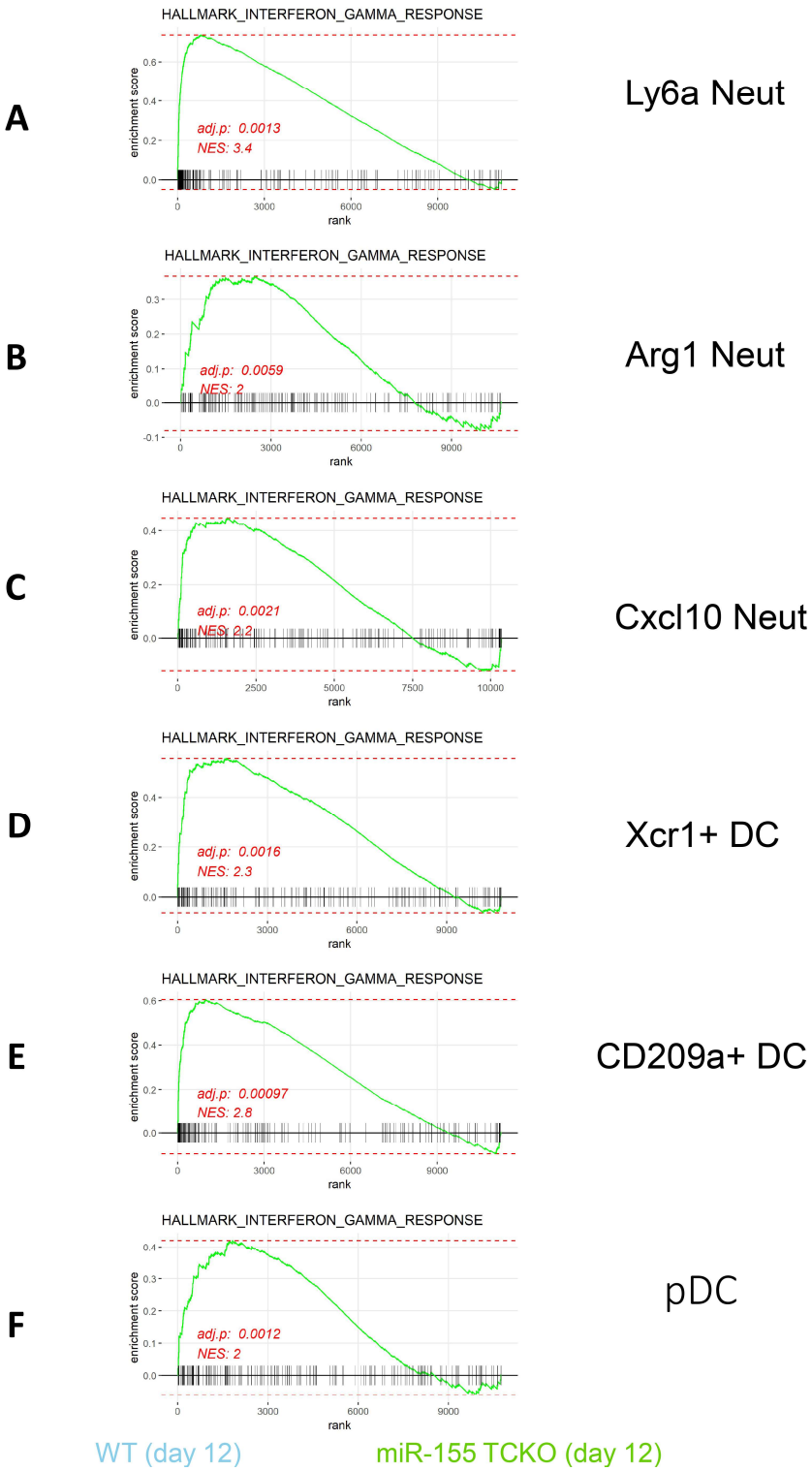

Figure S9 – IFNg response signature is enriched in multiple other myeloid cells in the WT TME. Significant enrichment was observed for **A.** Ly6a+ neutrophils, **B.** Arg1+ neutrophils, **C.** Cxcl10+ neutrophils, **D.** Xcr1+ DCs, **E.** CD209a+ DC, and F. pDCs. Data shown are derived from day 12. Normalized enrichment score (NES) and adjusted p values are shown.

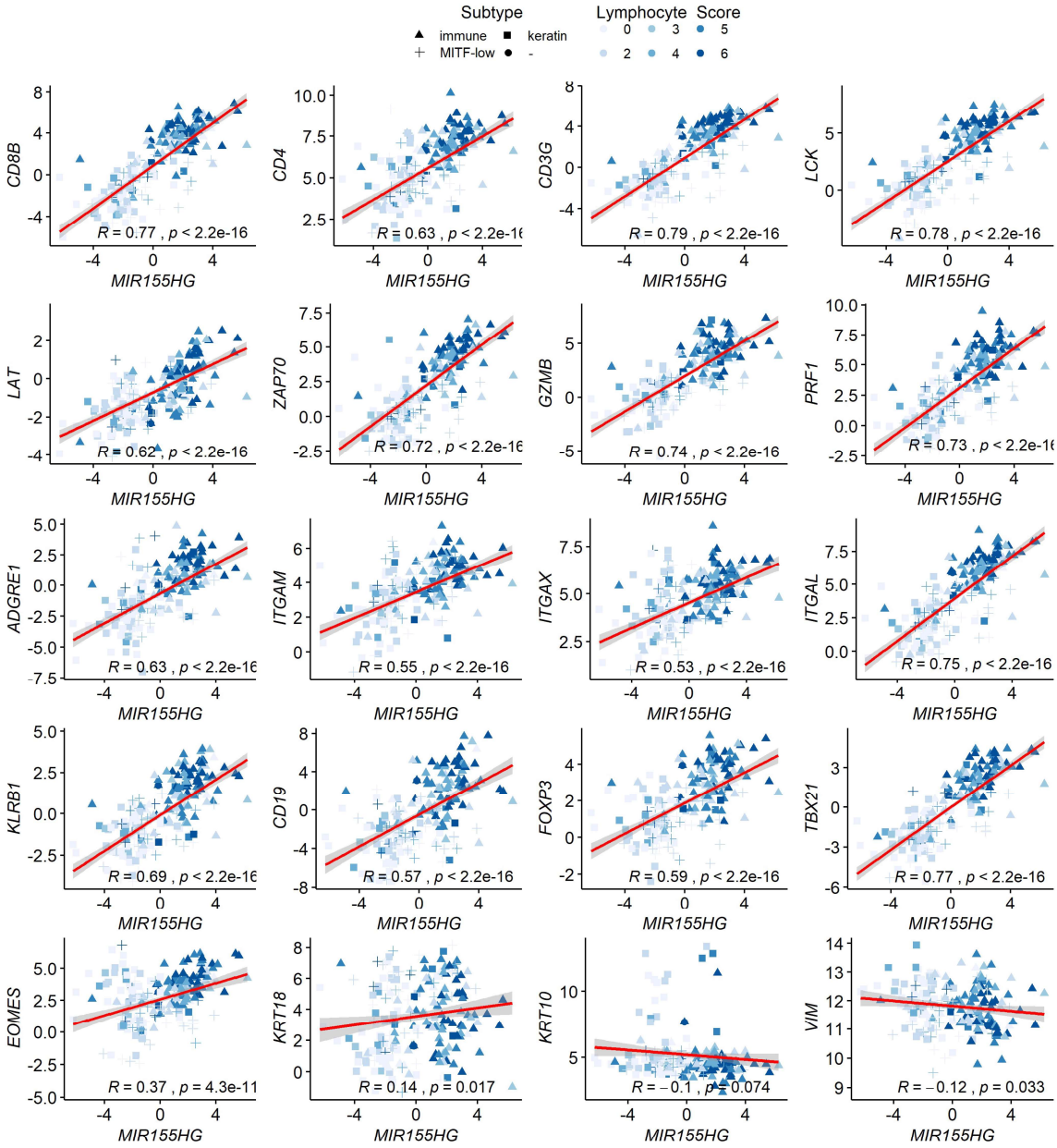

Figure S10 – *MIR155HG* expression correlates with immune-associated genes. Scatter plots showing the positive correlation between miR-155 host gene (*MIR155HG*) and immune-associated gene expression in TCGA-SKCM. Color gradient indicates the lymphocyte infiltration score of tumors, and the symbol shape indicates the molecular subtype of tumors (▲ Immune; ■ Keratin; + MITF-low; ● Uncategorized)

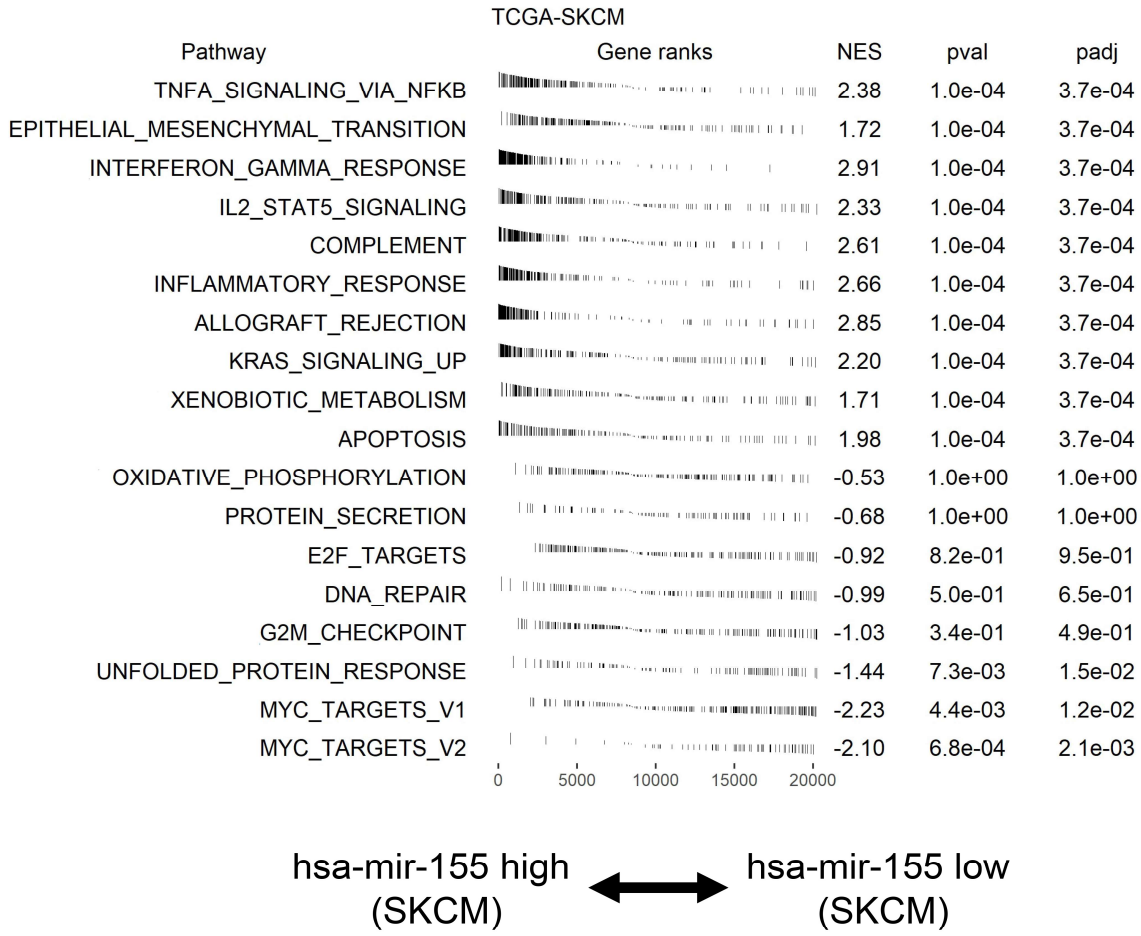

Figure S11 – Summary of GSEA analysis in TCGA-SKCM tumor subsets. Top 10 highly enriched gene sets in miR-155-high (left) and miR-155-low (right) subsets of SKCM tumors. Multiple immune pathways are enriched in miR-155-high tumor subsets whereas proliferative pathways were enriched in miR-155-low subsets.

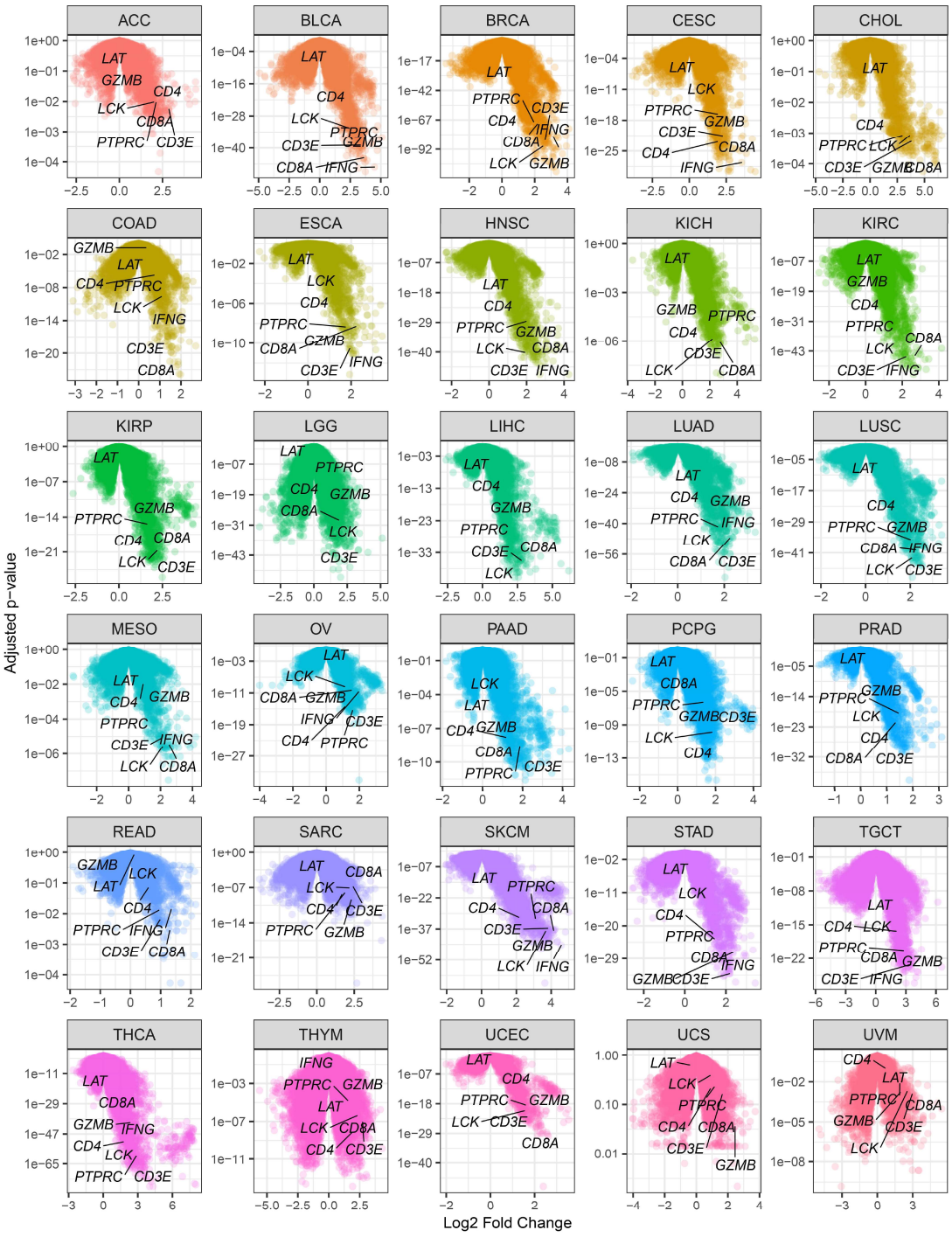

Figure S12 – High miR-155 expression marks an immune-enriched subtype in human solid tumors. Volcano plots showing differential expression levels of selected immune genes in miR-155-high subsets of TCGA tumors: ACC, Adrenocortical carcinoma; BLCA, Bladder Urothelial Carcinoma; LGG, Brain Lower Grade Glioma; BRCA, Breast invasive carcinoma; CESC, Cervical squamous cell carcinoma and endocervical adenocarcinoma; CHOL, Cholangiocarcinoma; COAD, Colon adenocarcinoma; ESCA, Esophageal carcinoma; HNSC, Head and Neck squamous cell carcinoma; KICH, Kidney Chromophobe; KIRC, Kidney renal clear cell carcinoma; KIRP, Kidney renal papillary cell carcinoma; LIHC, Liver hepatocellular carcinoma; LUAD, Lung adenocarcinoma; LUSC, Lung squamous cell carcinoma; MESO, Mesothelioma; OV, Ovarian serous cystadenocarcinoma; PAAD, Pancreatic adenocarcinoma; PCPG, Pheochromocytoma and Paraganglioma; PRAD, Prostate adenocarcinoma; READ, Rectum adenocarcinoma; SARC, Sarcoma; SKCM, Skin Cutaneous Melanoma; STAD, Stomach adenocarcinoma; TGCT, Testicular Germ Cell Tumors; THYM, Thymoma; THCA, Thyroid carcinoma; UCS, Uterine Carcinosarcoma; UCEC, Uterine Corpus Endometrial Carcinoma; UVM, Uveal Melanoma.

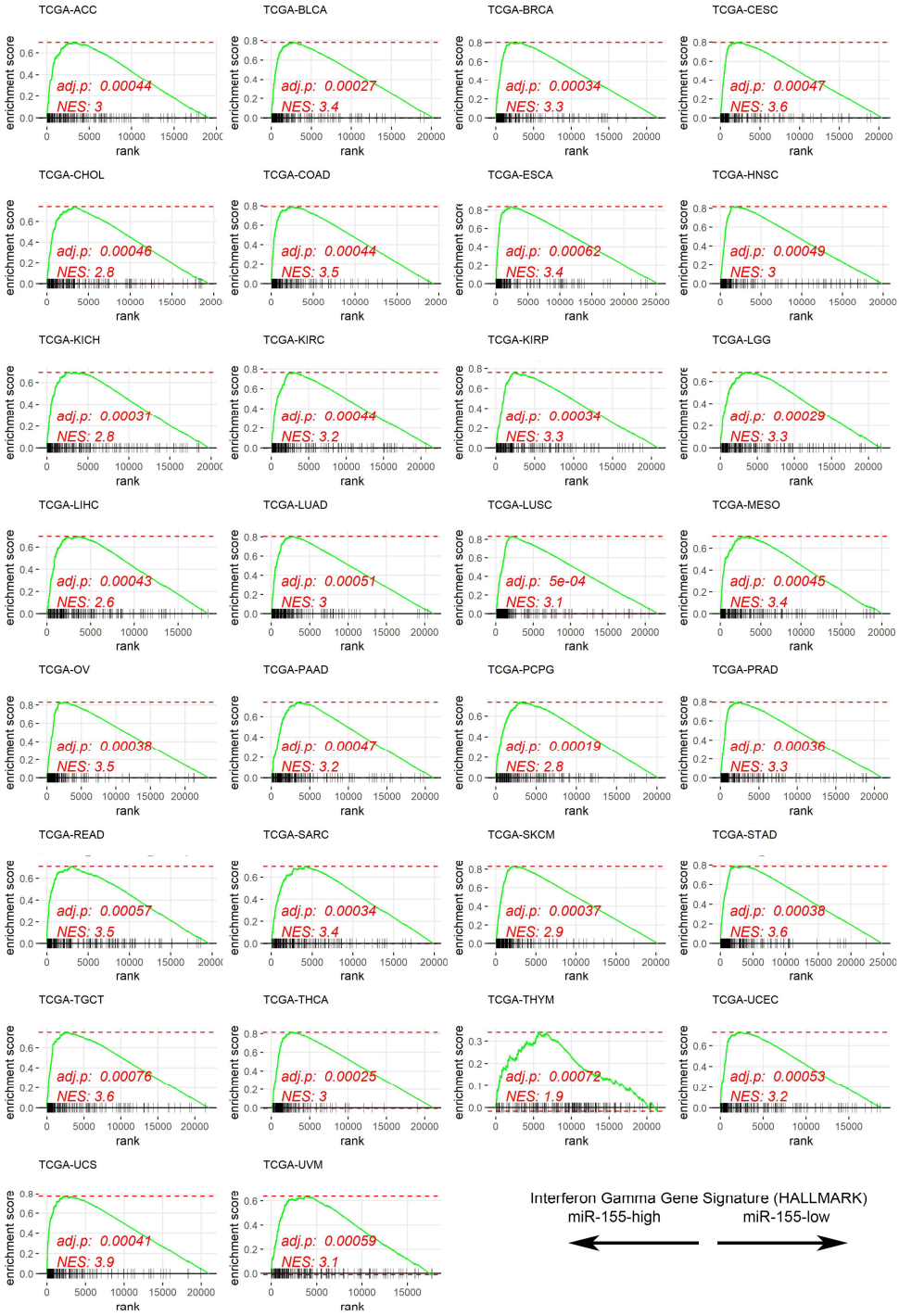

Figure S13 – miR155 expression in solid tumors is associated with an IFNg response signature. Analysis of the IFNg response gene signature in miR-155-high tumor subsets across TCGA cohorts. miR-155-high subsets of TCGA tumors (left side of the plot) were consistently defined by an enrichment of IFNg response signature suggesting an active immune component in the TME. Normalized enrichment score (NES) and adjusted p values are shown.

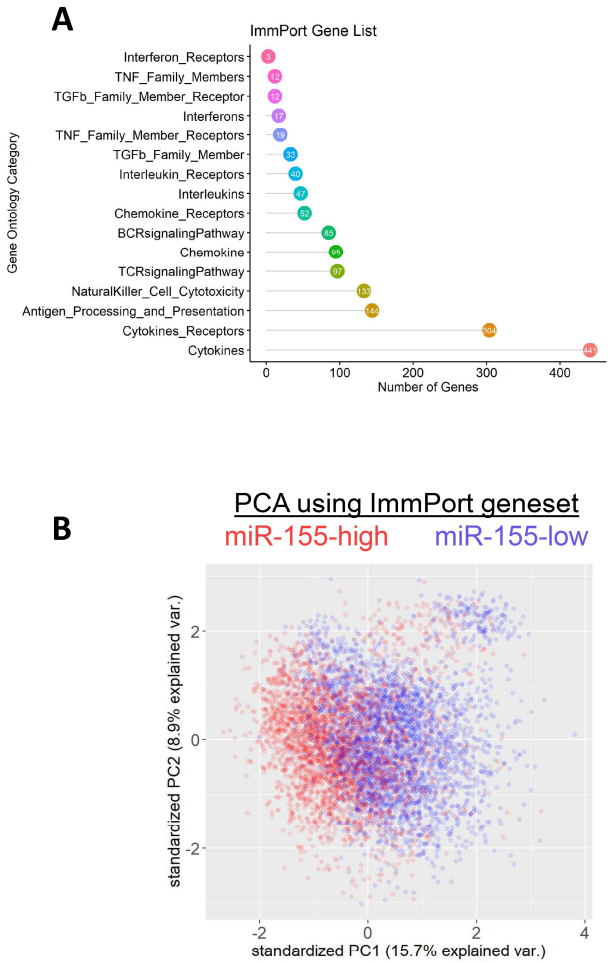

Figure S14 –Principal component analyses of gene expression in TCGA tumor cohorts. **A.** Gene class annotations of immune-related genes downloaded from the ImmPort database. **B.** PCA analysis of aggregated TCGA tumor cohorts using ImmPort genes (544 genes in analysis). Spatial separation of miR-155-high (red) tumors indicate miR-155 expression marks a similar immune gene expression profile among TCGA cancers.

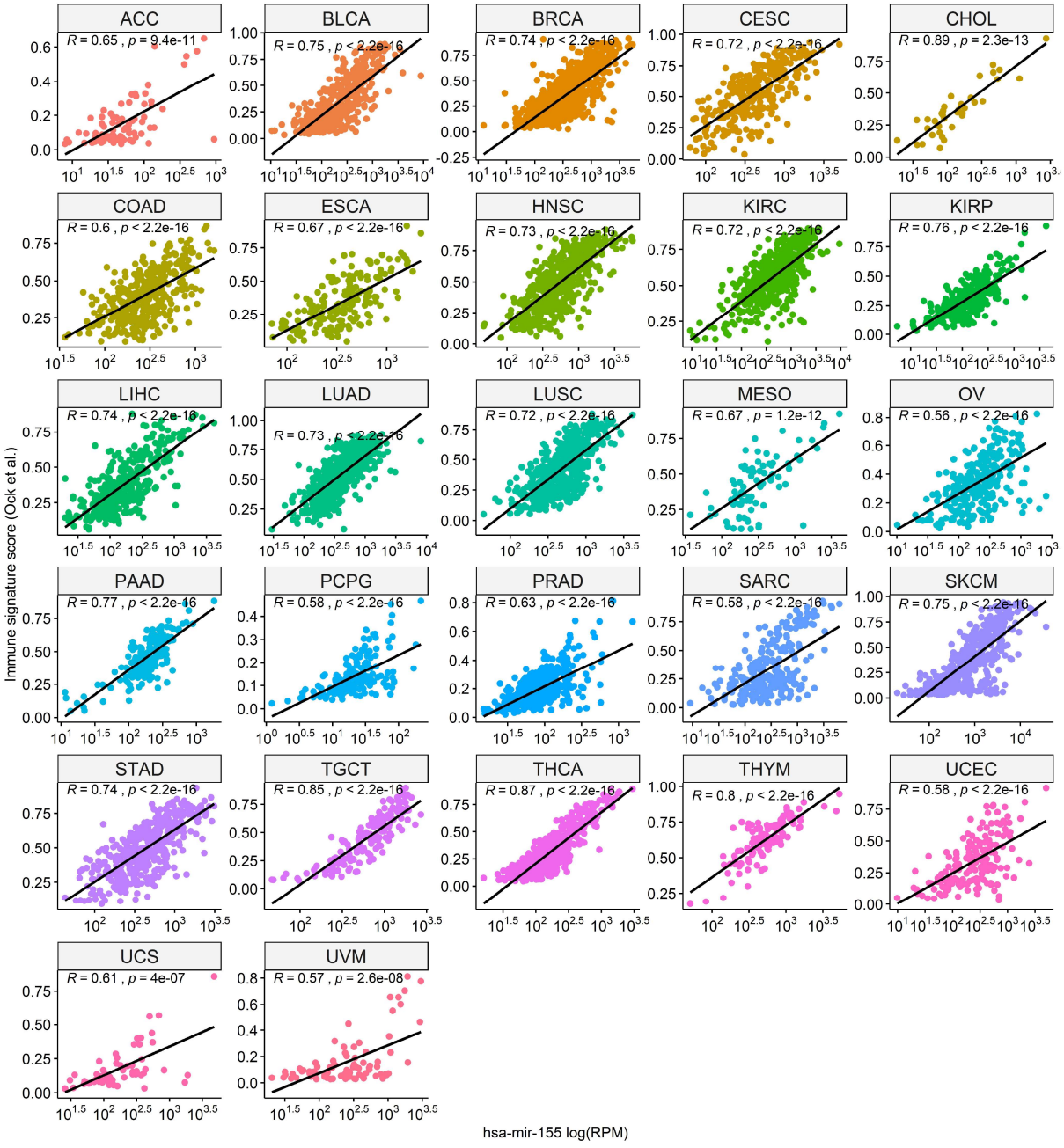

Figure S15 – miR-155 expression correlates with a predictor of immunotherapy response. miR-155 expression is strongly correlated with an immune signature score (IS score) (Ock et al. (1)) that predicts immunotherapy response. BLCA, Bladder Urothelial Carcinoma; LGG, Brain Lower Grade Glioma; BRCA, Breast invasive carcinoma; CESC, Cervical squamous cell carcinoma and endocervical adenocarcinoma; CHOL, Cholangiocarcinoma; COAD, Colon adenocarcinoma; ESCA, Esophageal carcinoma; HNSC, Head and Neck squamous cell carcinoma; KICH, Kidney Chromophobe; KIRC, Kidney renal clear cell carcinoma; KIRP, Kidney renal papillary cell carcinoma; LIHC, Liver hepatocellular carcinoma; LUAD, Lung adenocarcinoma; LUSC, Lung squamous cell carcinoma; MESO, Mesothelioma; OV, Ovarian serous cystadenocarcinoma; PAAD, Pancreatic adenocarcinoma; PCPG, Pheochromocytoma and Paraganglioma; PRAD, Prostate adenocarcinoma; READ, Rectum adenocarcinoma; SARC, Sarcoma; SKCM, Skin Cutaneous Melanoma; STAD, Stomach adenocarcinoma; TGCT, Testicular Germ Cell Tumors; THYM, Thymoma; THCA, Thyroid carcinoma; UCS, Uterine Carcinosarcoma; UCEC, Uterine Corpus Endometrial Carcinoma; UVM, Uveal Melanoma.

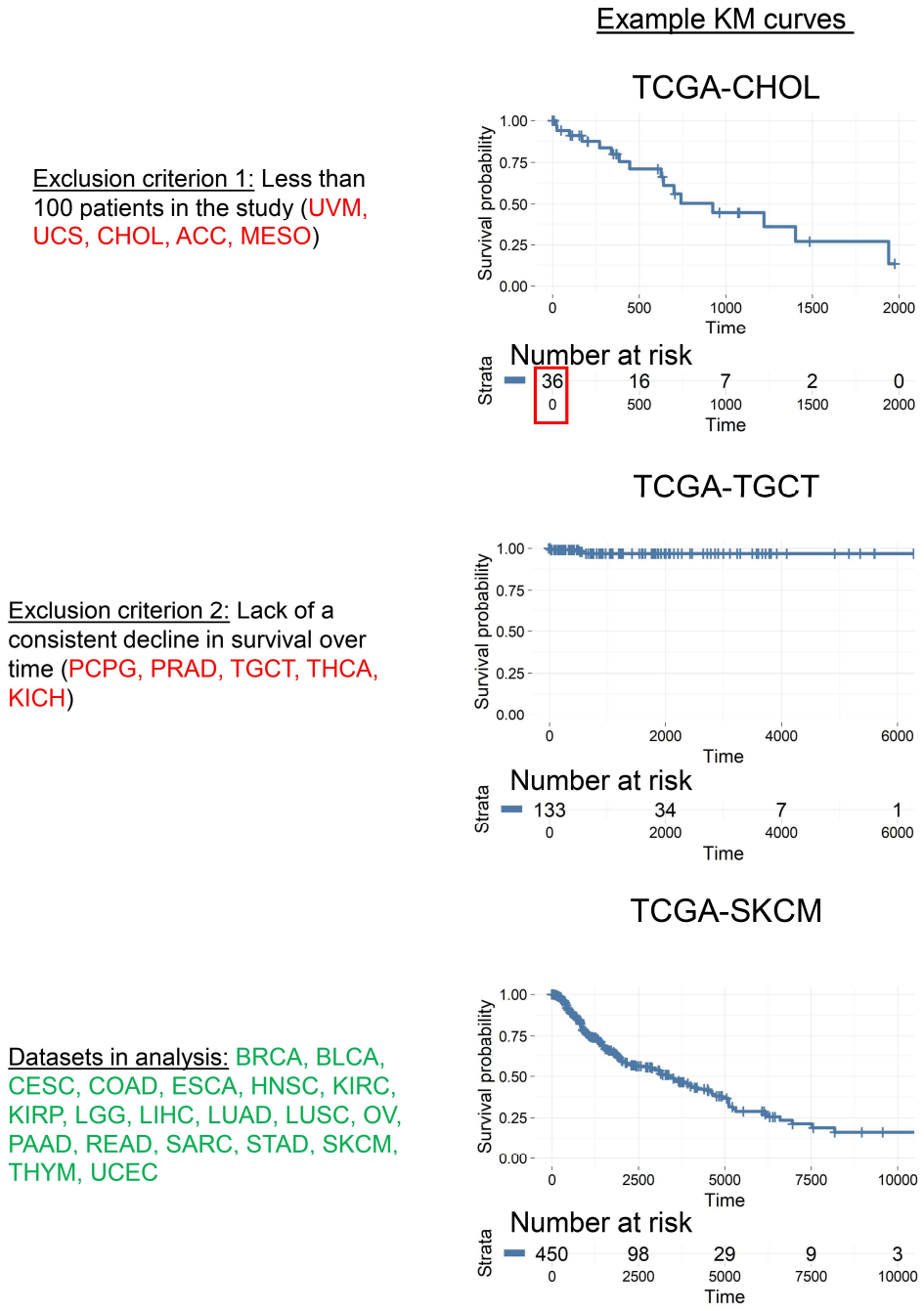

Figure S16 – Diagram showing the approach for including and excluding TCGA samples. The inclusion criteria for the analysis in Figure 6f are shown. Tumor types typed in red were excluded due to low (<100) numbers of patients or due to lack of a time-dependent decline in survival as evidenced by the uncategorized Kaplan-Meier (KM) curves. BLCA, Bladder Urothelial Carcinoma; LGG, Brain Lower Grade Glioma; BRCA, Breast invasive carcinoma; CESC, Cervical squamous cell carcinoma and endocervical adenocarcinoma; CHOL, Cholangiocarcinoma; COAD, Colon adenocarcinoma; ESCA, Esophageal carcinoma; HNSC, Head and Neck squamous cell carcinoma; KICH, Kidney Chromophobe; KIRC, Kidney renal clear cell carcinoma; KIRP, Kidney renal papillary cell carcinoma; LIHC, Liver hepatocellular carcinoma; LUAD, Lung adenocarcinoma; LUSC, Lung squamous cell carcinoma; MESO, Mesothelioma; OV, Ovarian serous cystadenocarcinoma; PAAD, Pancreatic adenocarcinoma; PCPG, Pheochromocytoma and Paraganglioma; PRAD, Prostate adenocarcinoma; READ, Rectum adenocarcinoma; SARC, Sarcoma; SKCM, Skin Cutaneous Melanoma; STAD, Stomach adenocarcinoma; TGCT, Testicular Germ Cell Tumors; THYM, Thymoma; THCA, Thyroid carcinoma; UCS, Uterine Carcinosarcoma; UCEC, Uterine Corpus Endometrial Carcinoma; UVM, Uveal Melanoma

Tumor	Mean miR-155 (log)	Cohort Size	Median Mutations (log)	Mutations per Mb (log)	Hazard Ratio	Lower 95% C.I. of HR	Upper 95% C.I. of HR	Coef.	Std Err (coef)	Z-score	Pr(>|z|)
LGG	1.53	511	2.94	-0.97	2.49	2.08	2.98	0.91	0.09	9.87	0.000
KIRC	2.86	339	3.78	-0.13	1.40	1.21	1.63	0.34	0.08	4.37	0.000
SKCM	3.23	758	5.72	1.80	0.84	0.76	0.93	-0.18	0.05	-3.43	0.001
PAAD	2.36	178	3.11	-0.80	1.41	1.07	1.85	0.34	0.14	2.44	0.015
CESC	2.78	305	4.19	0.28	0.73	0.56	0.95	-0.31	0.14	-2.31	0.021
LUSC	2.78	494	5.23	1.32	0.82	0.67	1.00	-0.20	0.10	-1.95	0.051
UCEC	2.68	542	4.36	0.44	0.82	0.67	1.01	-0.20	0.11	-1.88	0.060
HNSC	2.87	509	4.41	0.49	0.87	0.73	1.03	-0.14	0.09	-1.60	0.109
KIRP	2.31	288	3.97	0.06	1.29	0.94	1.77	0.25	0.16	1.58	0.113
READ	2.50	158	4.14	0.23	0.58	0.29	1.14	-0.55	0.35	-1.58	0.113
OV	2.50	443	4.28	0.36	0.91	0.80	1.03	-0.10	0.06	-1.54	0.125
SARC	2.74	255	3.43	-0.48	1.13	0.95	1.35	0.12	0.09	1.34	0.179
STAD	2.77	439	4.41	0.49	0.93	0.77	1.12	-0.07	0.09	-0.79	0.429
BRCA	2.68	1044	3.53	-0.39	0.93	0.77	1.12	-0.08	0.10	-0.79	0.430
LUAD	2.72	567	5.06	1.15	0.93	0.76	1.13	-0.07	0.10	-0.73	0.466
BLCA	2.62	412	4.88	0.97	0.95	0.82	1.10	-0.05	0.07	-0.70	0.482
LIHC	2.45	374	4.20	0.29	1.07	0.88	1.28	0.06	0.10	0.66	0.506
ESCA	2.67	184	4.44	0.53	1.10	0.81	1.49	0.10	0.15	0.62	0.532
COAD	2.55	433	4.33	0.42	1.01	0.78	1.31	0.01	0.13	0.10	0.923

Table S1 – Summary of univariate Cox proportional hazards analysis. miR-155 expression was used as a continuous variable for these analyses. miR-155 expression was not uniformly associated with an improved outcome in all the solid tumors analyzed. Tumors with two highest mutational burden, melanoma (SKCM) and squamous lung cancer (LUSC), exhibited a lower miR-155 hazard ratio.